

TOPICAL REVIEW - TOPOLOGICAL INSULATOR

# Topological edge states and electronic structures of a 2D topological insulator: Single-bilayer Bi (111)

To cite this article: Gao Chun-Lei *et al* 2013 *Chinese Phys. B* **22** 067304

View the [article online](#) for updates and enhancements.

## You may also like

- [Impurity effect on surface states of Bi \(111\) ultrathin films](#)  
Kai Zhu, , Dai Tian et al.
- [Ultrathin epitaxial Bi film growth on 2D HfTe<sub>2</sub> template](#)  
Evangelia Xenogiannopoulou, Dimitra Tsoutsou, Polychronis Tsipas et al.
- [Effect of staggered sublattice potential on electronic and transport properties of Bi\(111\) pristine and hydrogen-passivated nanoribbons](#)  
Mahfuzur Rahman Munna, Md Niloy Khan and Mahbub Alam

# Topological edge states and electronic structures of a 2D topological insulator: Single-bilayer Bi (111)\*

Gao Chun-Lei(高春雷)<sup>a)†</sup>, Qian Dong(钱冬)<sup>a)‡</sup>, Liu Can-Hua(刘灿华)<sup>a)</sup>,  
Jia Jin-Feng(贾金锋)<sup>a)</sup>, and Liu Feng(刘锋)<sup>b)</sup>

<sup>a)</sup>Key Laboratory of Artificial Structures and Quantum Control (Ministry of Education), Department of Physics, Shanghai Jiao Tong University, Shanghai 200240, China

<sup>b)</sup>Department of Materials Science & Engineering, University of Utah, Salt Lake City, Utah 84112, USA

(Received 20 April 2013)

Providing the strong spin-orbital interaction, Bismuth is the key element in the family of three-dimensional topological insulators. At the same time, Bismuth itself also has very unusual behavior, existing from the thinnest unit to bulk crystals. Ultrathin Bi (111) bilayers have been theoretically proposed as a two-dimensional topological insulator. The related experimental realization achieved only recently, by growing Bi (111) ultrathin bilayers on topological insulator  $\text{Bi}_2\text{Te}_3$  or  $\text{Bi}_2\text{Se}_3$  substrates. In this review, we started from the growth mode of Bi (111) bilayers and reviewed our recent progress in the studies of the electronic structures and the one-dimensional topological edge states using scanning tunneling microscopy/spectroscopy (STM/STS), angle-resolved photoemission spectroscopy (ARPES), and first principles calculations.

**Keywords:** topological insulators, edge states, electronic structures, Bi bilayer

**PACS:** 73.20.r, 74.25.Jb, 71.20.-b

**DOI:** 10.1088/1674-1056/22/6/067304

## 1. Introduction

Topological insulators (TIs) represent a new quantum phase of matter, with charge excitation gaps in the bulk and gapless Dirac cone edge states protected by time reversal symmetry at the edge.<sup>[1-5]</sup> The conception of TIs can be realized experimentally in three-dimensional (3D)<sup>[6-10]</sup> and two-dimensional (2D) materials.<sup>[11]</sup> One of the fundamental properties of the mobile electrons in the topological edge states is the spin-momentum locking that will be extremely useful in relation to possible applications in spintronics. In this sense, 2D TI can be advantageous over 3D TI in transport applications because electrons can only move along two well-defined directions in a 2D TI's 1D metallic edges. However, unlike the relatively rich family of 3D TI systems, in some sense, the HgTe/CdTe quantum well is the only well-defined 2D TI so far. Several other 2D TIs have been proposed. Among them, recently, ultrathin Bi (111) films draw both theoretical and experimental attention as a promising candidate 2D topological insulator (TI).<sup>[12-21]</sup> And the 2D topological properties of the ultra-thin Bi (111) films have been confirmed very recently.<sup>[17,18]</sup>

Experimental realization of ultrathin Bi (111) films, however, turns out to be quite difficult. Bismuth can be grown epitaxially with the unit of two atomic layers (bilayer (BL)).

On most substrates such as Si or graphene, Bi tends to grow as Bi (110) BLs in the ultrathin region and does not change to (111) direction before about 6 BLs.<sup>[12,22,23]</sup> This difficulty was overcome recently when single BL Bi (111) was successfully grown on 3D topological insulators  $\text{Bi}_2\text{Te}_3$  or  $\text{Bi}_2\text{Se}_3$  substrate.<sup>[17-21]</sup> STM/STS and ARPES experiments found the existence of one-dimensional edge states that reside in the 2D band gap and agree well with the theoretical prediction of the spatial distribution.<sup>[18]</sup> Besides its topological nature, single BL Bi (111) interfacing with TI can create a new Dirac cone in the bilayers due to a very strong Rashba-type spin-orbital interaction in the interface. This new Dirac cone can hybridize or non-hybridize with the original TI's Dirac cone, which causes unique behavior in this 2D/3D TIs heterostructure.

In this paper, we will review recent experimental and theoretical progress in the study of Bi (111) bilayer on  $\text{Bi}_2\text{Te}_3$  and  $\text{Bi}_2\text{Se}_3$  mostly based on our own results. The paper is organized as follows. After some general discussion of the growth method and spectroscopic measurement methods in Section 2, we show the electronic structures of single-bilayer Bi (111) and quasiparticle dynamics in Section 3. The study of the one-dimensional (1D) topological edge states is described in Section 4. The study of generating extrinsic spin-splitting Dirac

\*Project supported by the National Basic Research Program of China (Grants Nos. 2012CB927401, 2011CB921902, 2013CB921902, and 2011CB922200), the National Natural Science Foundation of China (Grants Nos. 91021002, 11174199, 11134008, and 11274228), and SCSTC (Grant Nos. 11JC1405000, 11PJ1405200, and 12JC1405300).

†Corresponding author. E-mail: [clgao@sjtu.edu.cn](mailto:clgao@sjtu.edu.cn)

‡Corresponding author. E-mail: [dqian@sjtu.edu.cn](mailto:dqian@sjtu.edu.cn)

like states in single-bilayer Bi is presented in Section 5. In the end (Section 6), we give conclusions and an outlook.

## 2. Growth of Bi (111) bilayers

$\text{Bi}_2\text{Te}_3$  and  $\text{Bi}_2\text{Se}_3$  thin films and bulk single crystals with different Fermi energies are used as substrates. Substrate films of up to 40 quintuple layers (QLs) are grown by molecular beam epitaxy (MBE) on Si (111) wafer.<sup>[24–27]</sup> Bulk single crystals are grown by a modified Bridgman method.<sup>[28–30]</sup> Single crystals were cleaved *in situ* at 10 K or room temperature, resulting in shiny, flat, and well-ordered surfaces. Bismuth films were grown on  $\text{Bi}_2\text{Te}_3$  and  $\text{Bi}_2\text{Se}_3$  substrates *in situ* at about 200 K. The thickness of Bi films was monitored by reflection high energy electron diffraction (RHEED) and further confirmed by STM. STM/STS measurements were carried out at 4.2 K. The sample temperature was kept at 100 K and/or 10 K during ARPES measurements which were performed with photon energy 9 eV–90 eV at Advanced Light Source (ALS) beamline 12.0.1 and the ARPES beamline in National Synchrotron Radiation Laboratory (NSRL, Hefei), using Scienta R4000 analyzers with base pressures better than  $5 \times 10^{-11}$ . Energy resolution is better than 15 meV and angular resolution is better than  $0.02 \text{ \AA}^{-1}$ .

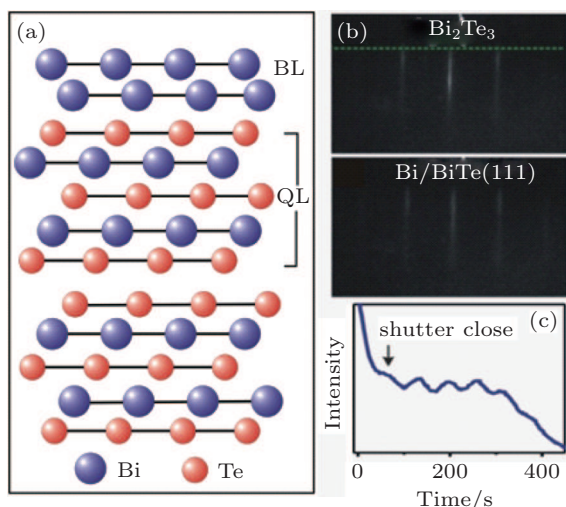


**Fig. 1.** (a) Structural model of Bi bilayer on  $\text{Bi}_2\text{Te}_3$ .  $\text{Bi}_2\text{Te}_3$  stacks in a quintuple layer and Bi stacks in bilayer fashion. (b) RHEED patterns before and after Bi deposition. (c) RHEED oscillations of Bi on  $\text{Bi}_2\text{Te}_3$ .<sup>[20]</sup>

Bismuth grows on  $\text{Bi}_2\text{Te}_3$  or  $\text{Bi}_2\text{Se}_3$  in the layer-by-layer mode with a minimum unit of one BL. Figure 1(a) gives a sketch of stacking of Bi bilayer on  $\text{Bi}_2\text{Te}_3$ . Bismuth adapts the lattice of the substrate  $\text{Bi}_2\text{Te}_3$  as can be seen from the nearly unchanged RHEED pattern before and after Bi deposition (Fig. 1(b)). The nicely layer-by-layer growth of Bi preserves up to at least 5 bilayers as shown by the RHEED oscillations in Fig. 1(c) with every oscillation representing the amount of one BL Bi. Careful analysis of the RHEED pattern shows a gradual lattice relaxation as the thickness of Bi

increases, which begins with the in-plane lattice constant of 4.386 (4.13)  $\text{\AA}$ , matching the lattice of  $\text{Bi}_2\text{Te}_3$  ( $\text{Bi}_2\text{Se}_3$ ), for one-bilayer Bi and stabilizes at  $4.45 \pm 0.05 \text{ \AA}$ , after 5 BLs.

The electronic structures change dramatically with the increase of Bi thickness due to quantum tunneling of electrons between the top and bottom surfaces,<sup>[14,15]</sup> it is crucial that any study of the desired thickness of Bi (111) is well controlled. In our studies, we mainly focus on single bilayer Bi (111), the shutter of the Bi source closes at the position of the first RHEED oscillation peak to get one-bilayer Bi film. Further, the coverage and morphology of the one-bilayer Bi is very carefully characterized by STM. Figure 2 shows topographic images of Bi (111) films at different coverages below 1 BL. The Bi (111) film first grows into individual triangular islands (Fig. 2(a)), and then the islands coalesce into a continuous BL film with triangle-like holes as the Bi coverage increases (Fig. 2(b)). Sharp and straight edges along (110) direction can be found for Bi (111) islands. An atomic-resolved STM image of the first BL Bi film is presented in Fig. 2(c). The hexagonal in-plane lattice is consistent with the Bi (111) orientation. The same in-plane lattice constant as the  $\text{Bi}_2\text{Te}_3$  or  $\text{Bi}_2\text{Se}_3$  substrate is confirmed in STM.

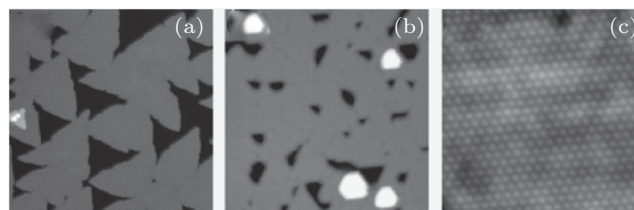


**Fig. 2.** STM images of Bi BL on  $\text{Bi}_2\text{Te}_3$ . (a) 0.7 BL, image size  $160 \text{ nm} \times 160 \text{ nm}$ . (b) 1.0 BL, image size  $50 \text{ nm} \times 50 \text{ nm}$ . (c) Atomically resolved images on Bi (111) BL, image size  $9 \text{ nm} \times 9 \text{ nm}$ .

## 3. Electronic states of single BL Bi (111) on $\text{Bi}_2\text{Te}_3$

Free standing single-BL Bi (111) is a semiconductor with a band gap of  $\sim 0.5 \text{ eV}$  according to the calculations.<sup>[14–16]</sup> When it was grown on  $\text{Bi}_2\text{Te}_3$  (111) substrate, Bi (111) bilayer created an exotic situation where the topologically protected one- and two-dimensional edge states coexist on the surface. It was first pointed out by Hirahara *et al.*<sup>[17]</sup> that an overlap of the band dispersions of BL Bi and  $\text{Bi}_2\text{Te}_3$  happens in  $\text{Bi}/\text{Bi}_2\text{Te}_3$  while preserving the helical Dirac cone of  $\text{Bi}_2\text{Te}_3$ .

The low energy band structures of the  $\text{Bi}_2\text{Te}_3$  substrates near the Fermi level around zone center ( $\Gamma$  point) are presented in Fig. 3(a). Linearly dispersive energy bands from surface states form a Dirac cone at the  $\Gamma$  point. In our films, the Dirac point can be located at  $\sim 0.2 \text{ eV}$  below Fermi level by extrapolating the “V”-shaped surface bands, which is consistent with previous experiments and calculations.<sup>[5,8,26]</sup> The electronic band structures change dramatically after being covered by a single BL Bi (111). Figures 3(b) and 3(c) presents

the ARPES spectra of single BL Bi/Bi<sub>2</sub>Te<sub>3</sub> along high symmetric directions. Seen from the spectra, the Bi<sub>2</sub>Te<sub>3</sub>'s bulk valence bands become invisible. Instead, two linearly dispersive bands cross at the  $\Gamma$  point at about 0.2 eV, which is near the location of the Dirac point of bare Bi<sub>2</sub>Te<sub>3</sub> film (Fig. 1(a)). Figure 3(d) shows the Fermi surface, which is totally different from that of bulk Bi (111).<sup>[12,14]</sup>

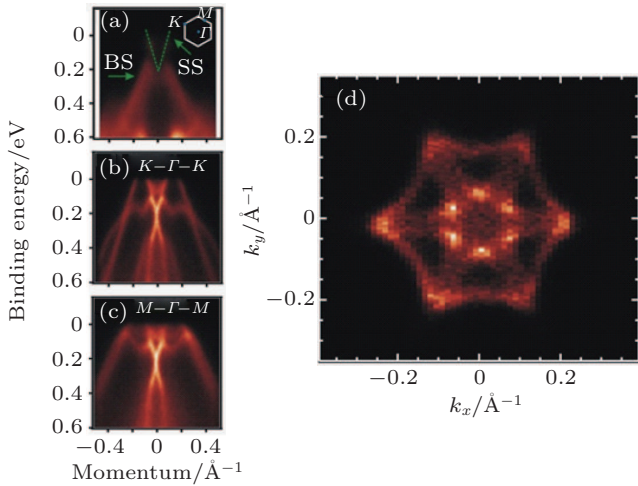


**Fig. 3.** (A) ARPES spectra of 40 QLs Bi<sub>2</sub>Te<sub>3</sub> film along  $K-\Gamma-K$  cut. Green lines mark the linearly dispersive “V” shape surface bands. The Dirac point is at the binding energy of  $\sim 0.2$  eV. The inset is the first surface Brillouin zone of the system.  $K$  and  $M$  are the highly symmetric points. (b) ARPES spectra of one-BL Bi (111) film on Bi<sub>2</sub>Te<sub>3</sub> along  $K-\Gamma-K$  and (c)  $M-\Gamma-M$  direction. (d) Fermi surface of single-BL Bi (111) on Bi<sub>2</sub>Te<sub>3</sub>.<sup>[20]</sup>

When exploring the region near the Dirac point by using higher ARPES resolution, supervising behavior was found. As presented in Figs. 4(a) and 4(b), we can see clearly that there is a vertical non-dispersive feature (about 50 meV in the energy scale) at the Dirac point. The upper “V”-shaped band and the lower “ $\Lambda$ ”-shaped band do not touch together directly as in a usual Dirac cone. The Fermi velocity of upper component and lower component of the new Dirac cone is about  $3.2 \times 10^5$  m/s and  $4.5 \times 10^5$  m/s. Further, the two-dimensional character of these unusual linearly dispersive bands was confirmed by photon energy-dependent experiments, as shown in Figs. 4(c)–4(d), which are widely used to separate surface states from bulk bands.<sup>[6]</sup> None of the observed dispersion relations of the linearly dispersive bands change, which indicates their 2D character. Relative intensity of the bands changes under different photon energy because of the photoemission matrix element effects and/or changing electron escape length.<sup>[32]</sup> The non-dispersive feature in a Dirac cone is a strong signature of a quasi-particle spectrum arising from some many-body interactions found in previous studies of graphene.<sup>[33–36]</sup> As a comparison, experimental band structures of single-BL Bi/Bi<sub>2</sub>Se<sub>3</sub> were shown in Fig. 5. There are two Dirac point-like band-crossing points marked as “ $D_{Bi}$ ” and “ $D_S$ ” in Fig. 5(b), while there is only one Dirac point in

bare Bi<sub>2</sub>Se<sub>3</sub> (Fig. 5(a)). Very different from Bi/Bi<sub>2</sub>Te<sub>3</sub>, no vertical features as seen in Fig. 4(a) are observed in Bi/Bi<sub>2</sub>Se<sub>3</sub>.

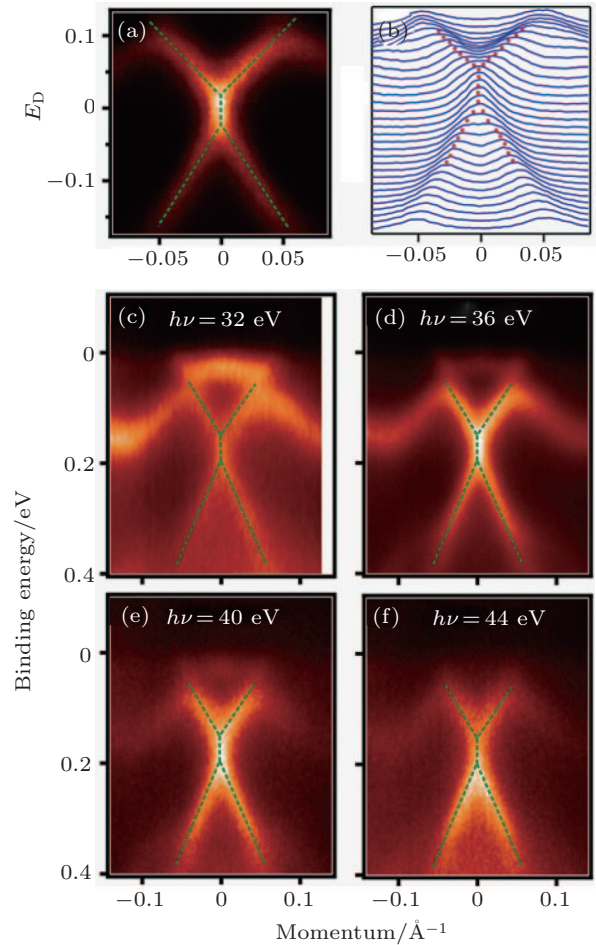


**Fig. 4.** (a) High resolution ARPES spectra near Dirac point and (b) the corresponding momentum distribution curves, (c) and (d) photon energy dependence of the ARPES spectra. Green lines mark the linearly dispersive bands and the non-dispersive feature.<sup>[20]</sup>

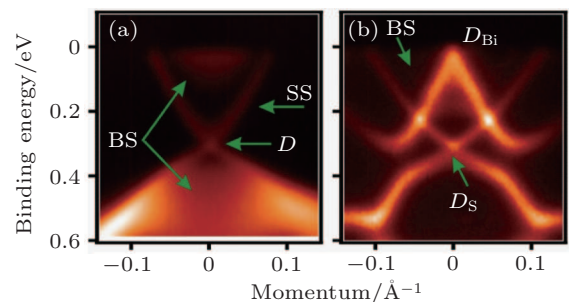


**Fig. 5.** (a) ARPES spectra of bulk Bi<sub>2</sub>Se<sub>3</sub> along  $K-\Gamma-K$  cut. The Dirac point “ $D$ ” is at the binding energy of  $\sim 0.3$  eV. (b) ARPES spectra of one BL Bi (111) film on Bi<sub>2</sub>Se<sub>3</sub> along  $K-\Gamma-K$ .<sup>[20]</sup>

To understand the origin of the electronic structures and the many-body behavior, we performed detailed density functional theory (DFT) calculations of the electronic band structures of Bi/Bi<sub>2</sub>Te<sub>3</sub> and Bi/Bi<sub>2</sub>Se<sub>3</sub>. Density functional theory calculations were carried out in the framework of the Perdew–Burke–Ernzerhof-type generalized gradient approximation using VASP package.<sup>[37]</sup> The lattice parameters of the substrate

were taken from experiments ( $a = 4.386 \text{ \AA}$  for  $\text{Bi}_2\text{Te}_3$ ,  $4.13 \text{ \AA}$  for  $\text{Bi}_2\text{Se}_3$ ), and the Bi bilayer is strained to match the substrate lattice parameter. All calculations are performed with a plane-wave cutoff of 600 eV on an  $11 \times 11 \times 1$  Monkhorst-Pack  $k$ -point mesh. The substrate is modeled by a slab of 6QL  $\text{Bi}_2\text{Te}_3$ , and the vacuum layers are over  $20\text{-\AA}$  thick to ensure decoupling between neighboring slabs. During structural relaxation, atoms in the lower 4QL substrate are fixed in their respective bulk positions, and the Bi bilayer and upper 2QL of substrate are allowed to relax until the forces are smaller than  $0.01 \text{ eV/\AA}$ .

Figures 6(a) and 6(b) show the calculated bands of Bi/ $\text{Bi}_2\text{Te}_3$ 's high symmetry directions. We only plot the spectra contributions from top Bi (111) bilayer. The brightness of the color presents the spectra weight. In comparison with experimental band structures, the observed ARPES spectra are consistent with the spectra from the top Bi (111) bilayer. Figure 6(c) shows the experimental bands overlaid with the calculated bands. We see that, overall, the agreement of band energies and dispersions between experiment and calculation is very good except for a slight shifting of the Fermi level. Figure 6(d) shows the spectra contributions from both the top Bi bilayer and the 2QLs of  $\text{Bi}_2\text{Te}_3$  beneath the Bi. The projected spectral function calculations show that the calculated Dirac cone " $D_h$ " at  $\sim 0.15 \text{ eV}$  below Fermi level (Figs. 6(a) and 6(b)) is a hybrid Dirac state between the Bi bilayer and the bulk  $\text{Bi}_2\text{Te}_3$  film, with  $\sim 50\%$  of the spectral weight coming from the Bi bilayer.

Figures 7(a) and 7(b) show the calculated energy bands of Bi/ $\text{Bi}_2\text{Se}_3$ . Spectra contribution from top Bi (111) bilayer is plotted in Fig. 7(a). Comparing the experimental data in

Fig. 6(b), we can easily see that the observed ARPES spectra are not purely from Bi layers. Figure 7(b) shows the spectra contributions from both the top Bi bilayer and the 2QLs of  $\text{Bi}_2\text{Se}_3$  beneath the Bi. The projected spectral function calculations show that there is very little hybridization between Bi and  $\text{Bi}_2\text{Se}_3$ . The calculated Dirac cone " $D_s$ " (Fig. 7(b)) is purely from the bulk  $\text{Bi}_2\text{Se}_3$ . " $D_{\text{Bi}}$ " comes from the Bi bilayer. Figure 7(c) shows the experimental bands overlaid with the calculated bands. The observed ARPES spectra are the total signals from Bi and  $\text{Bi}_2\text{Se}_3$ .

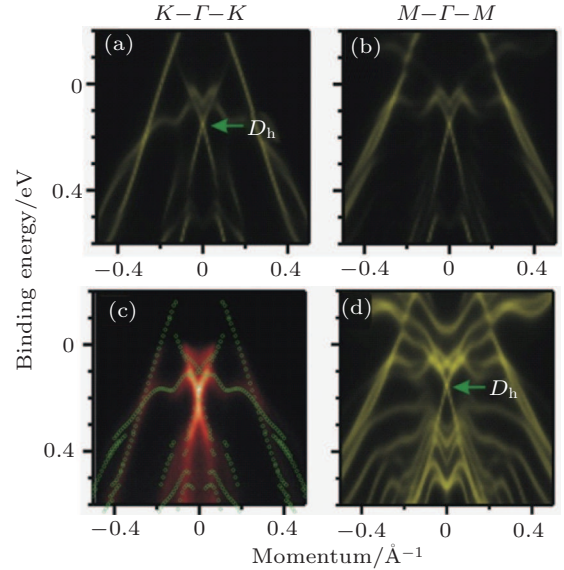


**Fig. 6.** (a) and (b) Calculated electronic bands from top Bi bilayer in Bi/ $\text{Bi}_2\text{Te}_3$  along two high symmetry directions. (c) Comparison of calculated bands and experimental results. (d) Contributions from top Bi bilayer plus upper 2QL  $\text{Bi}_2\text{Te}_3$ . The Bi bilayer has  $\sim 50\%$  spectral weight at the hybrid Dirac point ( $D_h$ ).<sup>[20]</sup>

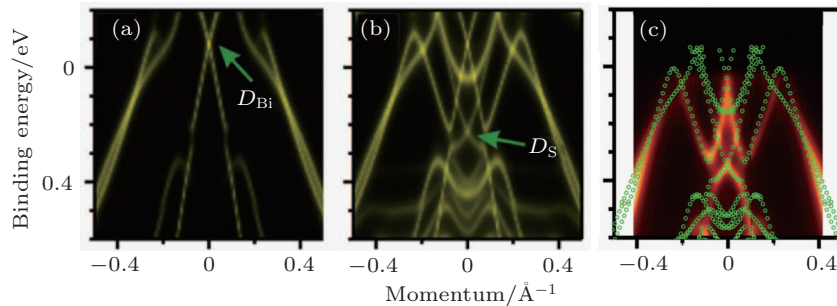


**Fig. 7.** Calculated electronic bands from (a) top Bi bilayer in Bi/ $\text{Bi}_2\text{Se}_3$ , (b) from top Bi bilayer plus upper 2QL  $\text{Bi}_2\text{Se}_3$  along  $M\text{-}\Gamma\text{-}M$  direction. (c) Comparison of calculated bands and experimental results.<sup>[20]</sup>

Setting aside for the moment the overall agreement between the DFT calculation and the ARPES experiment in band structure, there is a striking difference at the hybridized Dirac point in Bi/ $\text{Bi}_2\text{Te}_3$ . Single-particle DFT calculation's failure in reproducing the vertical features shown in Fig. 4(a) also indicates many-body behavior in this system. Based on ARPES data and band calculations, we reproduced the self-energy effect on the Bi/ $\text{Bi}_2\text{Te}_3$ . The projected spectral functions are cal-

culated through the equation

$$A_i(\mathbf{k}, \omega) = \frac{w_i(\mathbf{k})}{\pi} \frac{|\text{Im}\Sigma(\mathbf{k}, \omega)|}{[\omega - \varepsilon(\mathbf{k}) - \text{Re}\Sigma(\mathbf{k}, \omega)]^2 + [\text{Im}\Sigma(\mathbf{k}, \omega)]^2},$$

where  $\varepsilon$ ,  $\text{Re}\Sigma$ , and  $\text{Im}\Sigma$  are the single-particle band dispersions without many-body effects, and the real and imaginary parts of the self-energy, respectively. Label  $i$  denotes the atom index and  $w_i$  is the corresponding weight.  $\text{Im}\Sigma$  is extracted by the half-width of the experimental MDCs (Fig. 4(a)) multiplied by the band velocity.  $\text{Re}\Sigma$  is calculated from  $\text{Im}\Sigma$

through the Kramers–Kronig relations, and the full spectral function can be reconstructed using the calculated  $\text{Re}\Sigma$ . Figure 8 presents one MDC dataset. MDCs in “ $\Lambda$ ” bands can be fitted very well using two Lorentzian curves (Fig. 8(b)). Figure 8(c) shows the MDC width as a function of binding energy. The calculation is based on the data from 0.3 eV to 0.1 eV. Within this region, experimental band data can be well fitted to extract the width of momentum distribution curves (MDCs). Away from this region, Lorentzian peak fitting has large uncertainty due to the complexity of multiple bands. Actually, in our system, the error bar of the fitting results above  $\sim 0.2$  eV already becomes large. Beyond this region,  $\text{Im}\Sigma$  is set to be zero. Therefore, our theoretical self-energy extrac-

tion should be treated with caution, and the quantitative value of the self-energy correction will need to be done with much higher quality ARPES experiments. The aim of the theoretical fitting is to show the qualitative importance of self-energy correction in the Bi/Bi<sub>2</sub>Te<sub>3</sub> system. As shown in Figs. 8(d)–8(f), the non-dispersive vertical feature is nicely reproduced. Thus we believe there are many-body interactions in this hybridized Dirac cone. Based on comparing the results in Bi<sub>2</sub>Se<sub>3</sub>, we think the observed many-body interaction should be related with the strong hybridization between the Bi Dirac cone and TI’s Dirac cone; however, the exact form of many-body interaction needs to be further checked by experiments with much higher resolution.

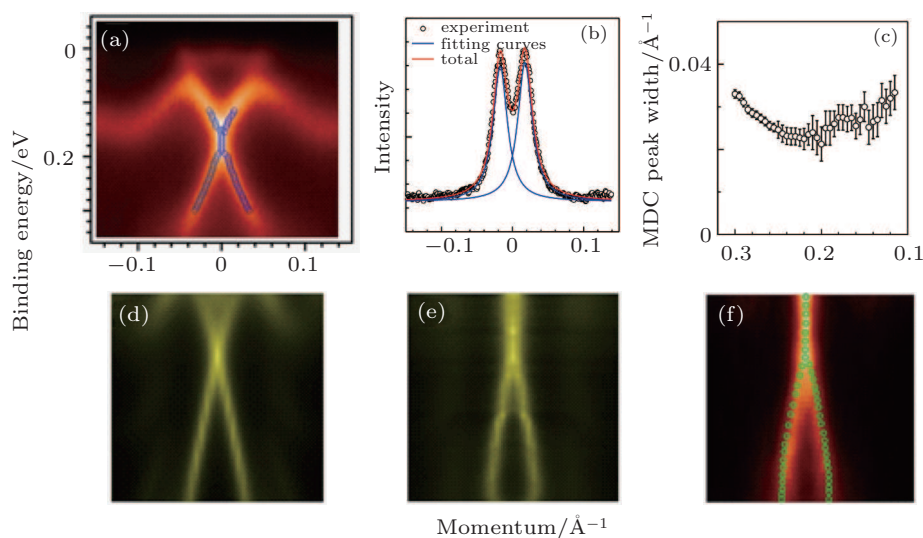


**Fig. 8.** (a) Band dispersion near Dirac cone. Blue open circles are the band dispersions extracted from MDC fitting. (b) MDC can be fitted very well using two Lorentzian curves. There could be two “indistinguishable” spectral lines within the vertical dispersion instead of one. But the half-width is the same using either one or two Lorentzian functions to fit. (c) MDC width as a function of binding energy. (d) LDA spectra without and (e) with the self-energy. (f) ARPES spectra overlaid by the calculation spectra of panel (e).<sup>[20]</sup>

#### 4. One-dimensional in-gap edge states of the Bi (111) bilayer

From the above results, we thoroughly understand the bulk electronic structures of the Bi (111) BL on substrate. Further, we studied the 1D edge states in the film. In 3D TIs, the existence of the topological surface states can be directly measured by APRES because those novel electrons are 2D states. However for 2D TIs, experimentally, the signals from 1D edge states are too weak to be directly observed by ARPES. Previous experiments on HgTe/CdTe rely on the transport measurements which are extremely difficult to make when the subjects are as small as the islands shown in Fig. 9(a). A plausible approach is STM/STS which can resolve the local density of states (LDOS) on the atomic scale. It has been proposed that the edge states of Bi (111) bilayer do not depend on the orientation or roughness of the step edge. In the experiment, however, to exclude the possible chemical and/or electrical interference at the meandering step edges, all the STS studies concentrate only on clean and sharp edges.

Figure 9 presents STS maps of 1 BL Bi (111) islands near the step edges on the clean Bi<sub>2</sub>Te<sub>3</sub>. The topography of single BL Bi (111)/Bi<sub>2</sub>Te<sub>3</sub> step is shown in Fig. 9(a) with Bi in the upper terrace and Bi<sub>2</sub>Te<sub>3</sub> in the lower terrace. Figure 9(b) shows the STS mapping where a bright feature along the step edge is clearly visible. This feature is sustained in the wide energy range from +136 mV to +370 mV, as shown in the line profiles of the STS maps in Fig. 9(c). The peak position of the bright feature, as marked the red dots, are essentially energy-independent within this energy window, which excludes the possibility of their standing wave origin. This bright feature is indeed an edge state that is spatially confined to the step edge and resides in a certain energy window.

The edge state shown in Fig. 9 spreads over several atomic rows with a  $\sim 2$ -nm width in real space. It is much wider than the normal electronic edge state, arising from edge dangling bonds or atomic reconstructions, and it is highly localized on the edge atoms in one or two lattices and decays exponentially away from the edge, much like the edge state

of graphene.<sup>[38,39]</sup> Note that the contribution of the chemical dangling bonds, even though present, cannot influence the feature nanometers away from step edge. The penetration depth of the topological edge states varies from a few to a few tens of nanometers depending on their  $k$ -space dispersion, which is different from material to material.<sup>[16,40]</sup> The wide spatial distribution in real space (relative to normal electronic edge state) indicates that these are likely topological edge states of 2D TIs. Further LDA calculation of the edge states of a free-standing Bi (111) BL nanoribbon, which is tensile-strained to the lattice constant of  $\text{Bi}_2\text{Te}_3$  shows that the width of the spatial distribution is  $k$ -point-dependent, ranging from  $\sim 0.7$  nm–2 nm.<sup>[18]</sup> At a given energy, the experimentally measured distribution has contributions from multiple  $k$ -points, giving rise to the observed width of several nanometers.

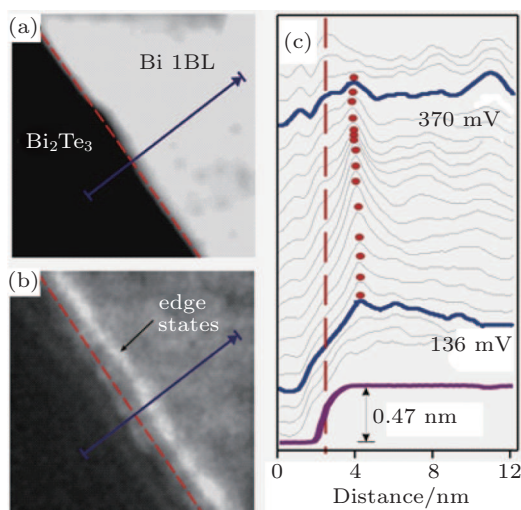


**Fig. 9.** (a) A typical clean and sharp step edge of Bi (111) BL on  $\text{Bi}_2\text{Te}_3$ . (b) The corresponding STS map at +283 mV. (c) Line profiles of topography and STS maps at various bias voltages. The red dashed lines mark the position of the step edge and red dots mark the position of edge states.<sup>[18]</sup>

Besides the unique spatial position, the 1D topological edge states are expected to reside inside the bulk gap of 2D TIs as well. Because the observed edge states in Bi (111) single bilayer are located above the Fermi level where no experimental data are available, we compare our STS data with the DFT band calculations. Figures 10(a) and 10(b) show the calculated bands of one-bilayer Bi on  $\text{Bi}_2\text{Te}_3$  substrate with a large energy scale and the ARPES results laid on the calculated bands. As also shown in Fig. 4, although the hybridization between the Bi layer and the  $\text{Bi}_2\text{Te}_3$  modified the band structure of free standing Bi (111), there is still an energy gap of 76 meV (Fig. 10(b)), slightly above the Fermi level. Within this energy gap, where the topological edge states should reside, figure 10(c) shows the  $dI/dV$  curves of the inner terrace (wide red rectangle in the inset) and the edge-state area (narrow blue rectangle in the inset) in the Bi (111) island. A proper

comparison of the STS data with the calculated band structure, however, needs a trustworthy alignment of the Fermi level.

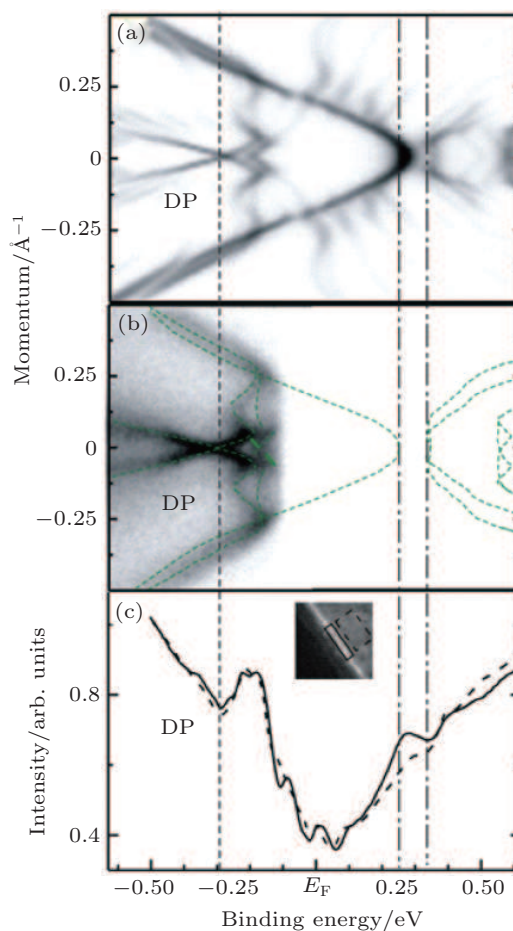


**Fig. 10.** (a) Calculated density of the electronic structure of Bi (111) BL on  $\text{Bi}_2\text{Te}_3$  ( $M-\Gamma-M$ ). (b) ARPES spectrum for one-bilayer Bi (111) on 40-QL together with the surface-originated bands taken from panel (a). (c) STS of the step edge (blue) and the inner terrace (red) of island averaged over the area as marked in the inset of panel (c). The STS, ARPES, and calculated bands are aligned by the Dirac point “DP,” as indicated by the dashed line. The dot-dashed lines mark the band gap of topmost Bi BL.<sup>[18]</sup>

In a previous STS study of a Dirac system, a dip in the  $dI/dV$  spectra due to the zero density of states at the Dirac point was observed.<sup>[41]</sup> In the Bi (111)/ $\text{Bi}_2\text{Te}_3$  system, there is a Dirac point in the Bi layer, and thus, we can align the dip feature in the STS spectra (Fig. 10(c)) to the calculated Dirac point (Fig. 10(a)), as marked by the dot-dashed vertical lines. After pinning down the Fermi level, we can locate the energy position of the edge states relative to the band gap position of Bi (111) single-BL. For the single-BL Bi/ $\text{Bi}_2\text{Te}_3$  step edge, in the energy window from +136 mV to +370 mV, intensity of the solid curve is noticeably higher than that of the dashed curve, which is exactly where the edge states are located (Fig. 9(c)). This also agrees well with the calculated band gap ( $\sim 76$  meV) of single-bilayer Bi/ $\text{Bi}_2\text{Te}_3$  film in Figs. 10(b) and 10(c), as marked by two dashed vertical lines. It is reasonable to expect that the STS attains higher contrast when STM scans over the edge state within the energy window of the band gap, where

the surface electronic states are absent and the edge electronic states are highly localized. The observed energy range of edge states is slightly larger than the band gap, possibly due to the energy extension of edge states in large  $k$ .<sup>[16]</sup> The fact that edge states are observed next to the step edge with a spatial distribution of several nanometers in real space and lies directly inside the 2D bulk band gaps in both cases provides unequivocal evidence that the single Bi (111) BL is a 2D TI. The edge state was also observed on single-BL Bi (111) islands on single-BL Bi (111)/Bi<sub>2</sub>Te<sub>3</sub>, but with a much smaller band gap (44 meV). The difference is caused by the change of the substrate. Obviously, the band structure of single-bilayer Bi (111) is strongly influenced by the substrate.

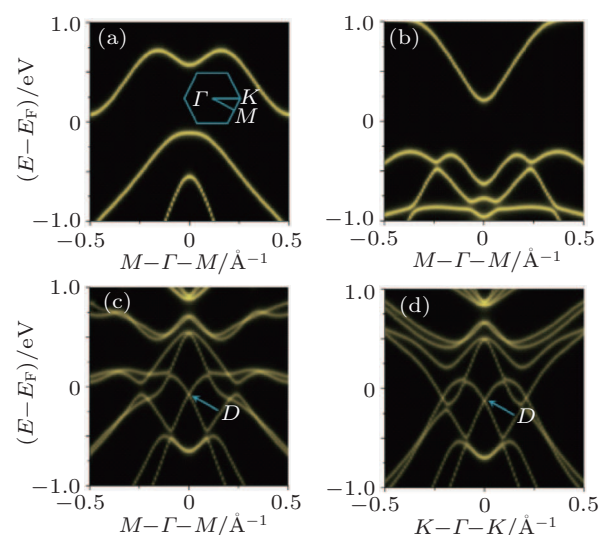
Another interesting issue is the thickness dependence of Bi (111)'s performance as a 2D topological insulator. There is a discrepancy in the theoretical predictions. Liu *et al.*<sup>[15]</sup> proposed that the Bi (111) retains the nontriviality of  $Z_2$  topological number up to 8 bilayers while Murakami<sup>[13]</sup> found that the nontriviality of the  $Z_2$  topological number holds only for odd bilayers, not for even bilayers. It would be interesting to check if the odd-even oscillation does exist experimentally. However, while the theoretical model is based on freestanding Bi (111) films, there is no real "freestanding" ultrathin film in experiments. A substrate is always needed which effectively alters the electronic structure of the Bi (111) layer. A plausible way to create semi-freestanding films is to grow Bi layer on insulating substrate which would expect a great reduction of the hybridization between adlayers and substrate. On the other hand, a more realistic model is needed for the theoretical calculation to further investigate the physical properties of Bi (111) ultrathin films.

## 5. Isolated Dirac-like spin-splitting states in single BL Bi (111) interfacing with single QL TIs

If the thickness of 3D TIs is reduced, the coupling between the up and down surface states will open an energy gap, eliminating the topological Dirac cone states; that is, linear dispersive bands revert to the parabolic conventional bands upon gap opening.<sup>[31,42,43]</sup> For example, when the thickness of Bi<sub>2</sub>Se<sub>3</sub> is reduced to less than six QLs, a gap opens.<sup>[31]</sup> And we know that single BL Bi (111) also has finite gap. It is known that when Bi grown on metal<sup>[44,45]</sup> or semiconductor substrates (for example, Si, Ge),<sup>[46,47]</sup> extrinsic helical Dirac-like surface state can be created by the substrate induced Rashba-type spin-splitting of Bi bands. However, there is always strong hybridization of surface and bulk states, and anyway, metal substrate is undesirable for device applications. We know from Section 3 that single-BL Bi (111) on Bi<sub>2</sub>Te<sub>3</sub> and Bi<sub>2</sub>Se<sub>3</sub><sup>[20]</sup> can have extrinsic formation of the helical Dirac states from Bi. Combining all these facts, we realized that the isolated extrinsic Dirac-like spin-splitting states in Bi can be

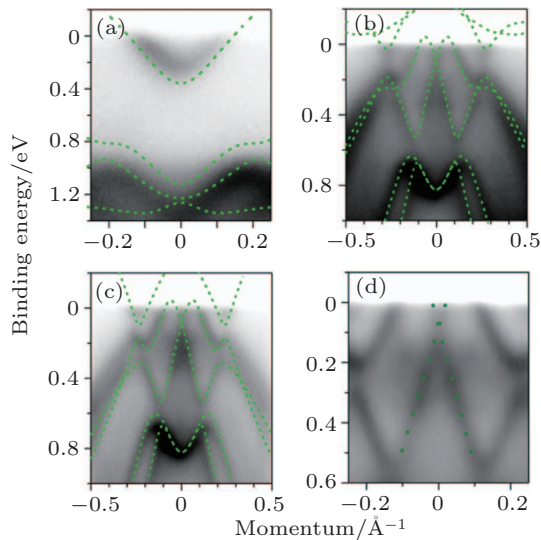
achieved by growing single BL Bi (111) on single QL Bi<sub>2</sub>Se<sub>3</sub> or Bi<sub>2</sub>Te<sub>3</sub>.<sup>[21]</sup>

Figure 11 shows the calculated low energy electronic bands for bare single-QL Bi<sub>2</sub>Se<sub>3</sub> (111) (Figs. 11(a) and 11(b)) and single-BL Bi (111) on single QL Bi<sub>2</sub>Se<sub>3</sub> (Figs. 11(c) and 11(d)). As shown in Fig. 11(b), we can clearly see an energy gap in 1QL Bi<sub>2</sub>Se<sub>3</sub>. After 1BL Bi (111) is deposited onto 1QL Bi<sub>2</sub>Se<sub>3</sub>, the band structures change dramatically. Most significantly, the gap vanishes as a linear dispersive band emerges around the  $\Gamma$  point to form the Dirac cone, marked with "D" in Figs. 11(c) and 11(d). The bands forming the Dirac cone are almost linear with the spin-momentum locking property, having a very large Fermi velocity, comparable to that in graphene or other TIs. Therefore, from charge and spin transport point of view, this ultra-thin heterostructure works equivalently well for possible spintronics device applications.



**Fig. 11.** Theoretical bands along the high-symmetry directions. (a) Bare Bi (111) BL along  $M-\Gamma-M$  direction at the bulk Bi<sub>2</sub>Se<sub>3</sub> lattice constant. Inset is the first Brillouin zone with highly symmetric points of  $\Gamma$ ,  $M$ , and  $K$ . (b) Bare 1QL Bi<sub>2</sub>Se<sub>3</sub> along  $M-\Gamma-M$  direction. (c) and (d) 1BL Bi (111) on 1QL Bi<sub>2</sub>Se<sub>3</sub> along  $M-\Gamma-M$  and  $K-\Gamma-K$  directions, respectively. The newly created Dirac cone is marked with "D". The relative intensity of bands at different  $k$ -points scales with the number of local density of states.<sup>[21]</sup>

The proposed films and band structures were successfully realized experimentally.<sup>[21]</sup> Figure 12 shows the ARPES spectra on 1 QL Bi<sub>2</sub>Se<sub>3</sub> and 1 BL Bi on 1 QL Bi<sub>2</sub>Se<sub>3</sub>. 1QL Bi<sub>2</sub>Se<sub>3</sub> substrates were grown first on graphene prepared on SiC wafer. An energy gap is observed for the bare 1QL Bi<sub>2</sub>Se<sub>3</sub> as shown in Fig. 12(a). In Figs. 12(b) and 12(c), the calculated bands are overlaid with the ARPES spectra along high symmetric directions. Obviously, the agreement between the theory and experiment is very good. The Dirac cone is isotropic. Figure 12(d) presents the high resolution ARPES spectra near the Dirac cone. Extracted from the data, the Fermi velocity of the Dirac cone in Bi is about  $6 \times 10^5$  m/s, which is very close to that of bare Bi<sub>2</sub>Se<sub>3</sub>.



**Fig. 12.** Comparison between experimental bands and the theoretical bands (a) Bare 1QL  $\text{Bi}_2\text{Se}_3$ . (b) and (c) 1BL Bi (111) on 1QL  $\text{Bi}_2\text{Se}_3$  along  $M-\Gamma-M$  and  $K-\Gamma-K$  directions, respectively. Green dashed lines are the theoretical bands. (d) High resolution ARPES spectra near the Dirac cone. Green dotted line marks the linearly dispersive bands that crossing at Dirac point at  $\sim 70$  meV below the Fermi level.<sup>[21]</sup>

We know from the calculation<sup>[21]</sup> that the Bi BL acts as a donor and the  $\text{Bi}_2\text{Se}_3$  as an acceptor. The charge transfer between them can generate a large internal electric field at the interface region, which can induce Rashba band splitting. The field intensity is estimated to be as high as  $\sim 1$  V/Å. The Rashba coupling constant is estimated to be  $\sim 4$  eV/Å. The spin-splitting Dirac-like states in Bi are extrinsically created by a giant Rashba effect due to the interfacial charge transfer.

## 6. Concluding remarks

We reviewed our recent progress in the experimental exploring of the topological properties as well the electric structures of single-bilayer Bi (111) films interfacing with TIs. In the last decades, Bi has kept providing us new quantum phenomenon related to its novel electronic states and large spin-orbital coupling. The topological properties of the single-bilayer Bi (111) is now much clearer than before, after extensive studies. However, the topological properties of thicker or bulk Bi are still a mystery and subject to lots of controversy. Improved sample quality and high resolution spectroscopic study may help us to get deeper and deeper insight into this fantastic element.

## References

[1] Hasan M Z and Kane C L 2010 *Rev. Mod. Phys.* **82** 3045  
 [2] Qi X L and Zhang S C 2011 *Rev. Mod. Phys.* **83** 1057  
 [3] Fu L and Kane C L 2007 *Phys. Rev. B* **76** 045302  
 [4] Bernevig B A, Hughes T L and Zhang S C 2006 *Science* **314** 1757  
 [5] Zhang H J, Liu C X, Qi X L, Dai X, Fang Z and Zhang S C 2009 *Nat. Phys.* **5** 438  
 [6] Hsieh D, Qian D, Wray L, Xia Y, Hor Y S, Cava R J and Hasan M Z 2008 *Nature* **452** 970

[7] Xia Y, Qian D, Hsieh D, Wray L, Pal A, Lin H, Bansil A, Grauer D, Hor Y S, Cava R J and Hasan M Z 2009 *Nat. Phys.* **5** 398  
 [8] Chen Y L, Analytis J G, Chu J H, Liu Z K, Mo S K, Qi X L, Zhang H J, Lu D H, Dai X and Fang Z 2009 *Science* **325** 178  
 [9] Hsieh D, Xia Y, Qian D, Wray L, Meier F, Dil J H, Osterwalder J, Patthey L, Fedorov A V, Lin H, Bansil A, Grauer D, Hor Y S, Cava R J and Hasan M Z 2009 *Phys. Rev. Lett.* **103** 146401  
 [10] Wang M X, Liu C H, Xu J P, Yang F, Miao L, Yao M Y, Gao C L, Shen C Y, Ma X C, Chen X, Xu Z A, Liu Y, Zhang S C, Qian D, Jia J F and Xue Q K 2012 *Science* **336** 52  
 [11] Koening M, Wiedmann S, Bruene C, Roth A, Buhmann H, Molenkamp L W, Qi X L and Zhang S C 2007 *Science* **318** 766  
 [12] Hofmann Ph 2006 *Prog. Surf. Sci.* **81** 191  
 [13] Murakami S 2006 *Phys. Rev. Lett.* **97** 236805  
 [14] Koroteev Yu M, Bihlmayer G, Chulkov E V and Bluegel S 2008 *Phys. Rev. B* **77** 045428  
 [15] Liu Z, Liu C X, Wu Y S, Duan W H, Liu F and Wu J 2011 *Phys. Rev. Lett.* **107** 136805  
 [16] Wada M, Murakami S, Freimuth F and Bihlmayer G 2011 *Phys. Rev. B* **83** 121310  
 [17] Hirahara T, Bihlmayer G, Sakamoto Y, Yamada M, Miyazaki H, Kimura S I, Blügel and Hasegawa S 2011 *Phys. Rev. Lett.* **107** 166801  
 [18] Yang F, Miao L, Wang Z F, Yao M Y, Zhu F F, Song Y R, Wang M X, Xu J P, Fedorov A V, Sun Z, Zhang G B, Liu C H, Liu F, Qian D, Gao C L and Jia J F 2012 *Phys. Rev. Lett.* **109** 016801  
 [19] Xiao S, Wei D and Jin X F 2012 *Phys. Rev. Lett.* **109** 166805  
 [20] Miao L, Wang Z F, Ming W M, Yao M, Wang M, Yang F, Song Y R, Zhu F F, Fedorov A, Sun Z, Gao C L, Liu C, Xue Q K, Liu C X, Liu F, Qian D and Jia J F 2013 *Proceedings of the National Academy of Sciences of the United States of America (PNAS)* **110** 2758  
 [21] Wang Z F, Yao M Y, Ming W M, Miao L, Zhu F F, Liu C H, Gao C L, Qian D, Jia J F and Liu F 2013 *Nature Commun.* **4** 1384  
 [22] Nagao T, Sadowski J T, Saito M, Yaginuma S, Fujikawa Y, Kogure T, Ohno T, Hasegawa Y, Hasegawa S and Sakurai T 2004 *Phys. Rev. Lett.* **93** 105501  
 [23] Hirahara T, Nagao T, Matsuda I, Bihlmayer G, Chulkov E V, Koroteev Y M, Echenique P M, Saito M and Hasegawa S *Phys. Rev. Lett.* **97** 146803  
 [24] Jia J F, Ma X C, Chen X, Sakurai T and Xue Q K 2011 *J. Phys. D: Appl. Phys.* **44** 464007  
 [25] Li Y Y, Wang G, Zhu X G, Liu M H, Ye C, Chen X, Wang Y Y, He K, Wang L L, Ma X C, Zhang H J, Dai X, Fang Z, Xie X C, Liu Y, Qi X L, Jia J F, Zhang S C and Xue Q K 2010 *Adv. Mater.* **22** 4002  
 [26] Wang G, Zhu X G, Sun Y Y, Li Y Y, Zhang T, Wen J, Chen X, He K, Wang L L, Ma X C, Jia J F, Zhang S B and Xue Q K 2011 *Adv. Mater.* **23** 2929  
 [27] Zhang T, Cheng P, Chen X, Jia J F, Ma X C, He K, Wang L L, Zhang H J, Dai X, Fang Z, Xie X C and Xue Q K 2009 *Phys. Rev. Lett.* **103** 266803  
 [28] Hor Y S, Roushan P, Beidenkopf H, Seo J, Qu D, Checkelsky J G, Wray L A, Hsieh D, Xia Y, Xu S Y, Qian D, Hasan M Z, Ong N P, Yazdani A and Cava R J 2010 *Phys. Rev. B* **81** 195203  
 [29] Song Y R, Yang F, Yao M, Zhu F, Miao L, Xu J, Wang M, Li H, Yao X, Ji F, Qiao S, Sun Z, Zhang G B, Gao B, Liu C, Qian D, Gao C L and Jia J F 2012 *Appl. Phys. Lett.* **100** 242403  
 [30] Li H, Song Y R, Yao M Y, Yang F, Miao L, Zhu F F, Liu C H, Gao C L, Qian D, Yao X, Jia J F, Shi Y J and Wu D 2012 *Appl. Phys. Lett.* **101** 072406  
 [31] Zhang Y, He K, Chang C, Song C, Wang L, Chen X, Jia J F, Fang Z, Dai X, Shan W Y, Shen S Q, Niu Q, Qi X L, Zhang S C, Ma X C and Xue Q K 2010 *Nat. Phys.* **6** 584  
 [32] Damascelli A, Hussain Z and Shen Z X 2003 *Rev. Mod. Phys.* **75** 473  
 [33] Bostwick A, Ohta T, Seyller T, Horn K and Rotenberg E 2007 *Nat. Phys.* **3** 36  
 [34] Bostwick A, Speck F, Seyller T, Horn K, Polini M, Asgari R, MacDonald A H and Rotenberg E 2010 *Science* **328** 999  
 [35] Siegel D A, Park C H, Hwang C Y, Deslippe J, Fedorov A V, Louie S G and Lanzara A 2011 *Proceedings of the National Academy of Sciences of the United States of America (PNAS)* **108** 11365  
 [36] Walter A L, Bostwick A, Jeon K J, Speck F, Ostler M, Seyller T, Moreschini L, Chang Y J, Polini M, Asgari R, MacDonald A H, Horn K and Rotenberg E 2011 *Phys. Rev. B* **84** 085410

- [37] Kresse G and Hafner J 1993 *Phys. Rev. B* **47** 558
- [38] Yu D, Lupton E M, Liu M, Liu W and Liu F 2008 *Nano Res.* **1** 56
- [39] Tao C and Jiao L, *et al.* 2011 *Nat. Phys.* **7** 616
- [40] Lai K, Kundhikanjana W, Kelly M A, Shen Z X, Shabani J and Shayegan M 2011 *Phys. Rev. Lett.* **107** 176809
- [41] Cheng P, Song C, Zhang T, Zhang Y, Wang Y, Jia J F, Wang J, Wang Y Y, Zhu B F, Chen X, Ma X C, He K, Wang L, Dai X, Fang Z, Xie X C, Qi X L, Liu C X, Zhang S C and Xue Q K 2010 *Phys. Rev. Lett.* **105** 076801
- [42] Park K, Heremans J J, Scarola V W and Minic D 2010 *Phys. Rev. Lett.* **105** 186801
- [43] O V, Moore J E and Louie S G 2010 *Phys. Rev. Lett.* **105** 266806
- [44] Ast C R, Henk J, Ernst A, Moreschini L, Falub M C, Pacilé D, Bruno P, Kern K and Grioni M 2007 *Phys. Rev. Lett.* **98** 186807
- [45] Mathias S, Ruffing A, Deicke F, Wiesenmayer M, Sakar I, Bihlmayer G, Chulkov E V, Koroteev Yu M, Echenique P M, Bauer M and Aeschlimann M 2010 *Phys. Rev. Lett.* **104** 066802
- [46] Gierz I, Suzuki T, Frantzeskakis E, Pons S, Ostanin S, Ernst A, Henk J, Grioni M, Kern K and Ast C R 2009 *Phys. Rev. Lett.* **103** 046803
- [47] Ohtsubo Y, Hatta S, Yaji K, Okuyama H, Miyamoto K, Okuda T, Kimura A, Namatame H, Taniguchi M and Aruga T 2010 *Phys. Rev. B* **82** 201307